A COMPARISON OF EXTERNAL ARRAY SELF-CALIBRATION ALGORITHMS USING EXPERIMENTAL DATA

Hasan S. Mir

University of Washington, Seattle
hmir@ee.washington.edu

Catherine M. Keller

MIT Lincoln Laboratory
keller@ll.mit.edu

ABSTRACT

Two recently published external array self-calibration algorithms are applied to experimental data obtained using a surveyed 12-element large sparse aperture array operating at 980 MHz. Though the algorithms are similar in that they use iterative methods to attempt to estimate the angle-of-arrival (AOA) of incoming signals with an imperfectly calibrated array, they are formulated quite differently. The performances of these algorithms are evaluated through their ability to reduce spurious peaks in direction finding (DF) spectra and accurately estimate the AOA of an incoming signal.

1. INTRODUCTION

Direction finding (DF) algorithms based on eigenstructure methods (such as MuSIC), utilize an underlying model which presumes a coherent phase relationship among the antenna array elements. Such a relationship almost never occurs in practice due to various antenna effects such as antenna pattern differences and antenna-to-receiver electrical cable length differences. Array calibration is required to establish the coherent phase relationship.

External array calibration is performed to compensate for array anomalies by attempting to fit the actual array response to an assumed theoretical response model. For a sparse aperture array in which antenna mutual coupling is not an issue, the fit achieved by applying an appropriate complex gain to each array antenna is usually sufficient. Typically, multiple signals with different AOAs in the array coverage area are used to derive a single solution for AOA-independent complex calibration gains.

During the last decade, increasing attention has been paid to external array calibration in the specific context of self-calibration algorithms. Self-calibration algorithms can be formulated for a wide variety of scenarios. The chief concern of this paper is with situations in which a surveyed but imperfectly calibrated antenna array is used to perform DF on an unsurveyed source. The practical application of interest is one in which nominal array calibration has been established and self-calibration is used on signals of opportunity to update the calibration.

This work was sponsored by the Department of Defense under Air Force Contract F19628-00-C-0002. Opinions, interpretations, conclusions, and recommendations are those of the authors and are not necessarily endorsed by the United States Air Force.

In most published works, the performance of self-calibration algorithms is evaluated via simulation only [2]-[3]. In this paper, the results of the two recently published self-calibration algorithms (Flieller [1] and Manikas [2]) are complemented by an examination of their effectiveness on experimental data described in [4].

This paper is organized as follows. Section 2 describes the experimental setup used to collect the data. Section 3 summarizes the self-calibration algorithms that are to be examined. Section 4 presents the results of running the self-calibration algorithms on the experimental data. Section 5 summarizes the results.

2. EXPERIMENTAL SETUP

The experimental data used for this work was taken at 980 MHz on a 12-element large sparse aperture array, located on the roof of a four-story garage in Cambridge, MA. The array configuration is shown in Figure 2(a). The array beamwidth is approximately $1.37°$. Each calibration source transmitted using a directional horn antenna from a line-of-sight location. Though data was collected for calibration sources with different AOAs, results are provided in this paper for data collected using the first source only, since similar results are obtained using the other sources. The location of the first source relative to the array is shown in Figure 2(b). To obtain a propagation channel with insignificant multipath, the source locations were placed in the near field of the array. Thus, the calibration algorithms are modified to accommodate a spherical wavefront.

Prior to conducting the experiment, the array and source locations were precisely surveyed so that actual AOAs could be compared to the output of the self-calibration algorithms for the purpose of performance evaluation. Also, complex calibration gains were computed using the surveyed sources and array as described in Section 3 of [4] to establish a nominally calibrated array response. Then, to evaluate the self-calibration algorithms, phase errors are introduced to each element of the nominal response via simulation.

3. SELF-CALIBRATION ALGORITHMS

Both algorithms are evaluated for the situation in which the array is surveyed with known antenna locations, but significant calibration errors exist and the source location is not known. The following are brief interpretations of the self-calibration algorithms examined.

3.1. Self-Calibration Algorithm of Flieller [1]

This algorithm is similar to the algorithm of Weiss and Friedlander [3], except that the regularization term $(\delta-\delta_N)^H\Psi^{-1}(\delta-\delta_N)$, where δ_N is the nominal complex gain vector and Ψ is the corresponding covariance matrix, has been added to the MuSIC cost function so that it takes on the form of a MAP estimator. The regularization term increases the robustness of the algorithm to large perturbations of the complex gains. Optimization of the modified cost function results in a pair of one-dimensional functions given by

$$\delta_k = \left(\mathbf{Q}(\theta)+\Psi^{-1}\right)^{-1}\Psi^{-1}\delta_{k-1} \quad (1)$$

$$f_k(\theta) = \delta_{k-1}^H\Psi^{-1}\left(\Psi-\left(\mathbf{Q}(\theta)+\Psi^{-1}\right)^{-1}\right)\Psi^{-1}\delta_{k-1} \quad (2)$$

where $\mathbf{Q}(\theta)\stackrel{\triangle}{=}\text{diag}(\mathbf{A}(\theta))^H\hat{\Pi}_n\text{diag}(\mathbf{A}(\theta))$, $\mathbf{A}(\theta)$ is the array response vector, and $\hat{\Pi}_n$ is the estimated noise subspace projection. The algorithm iterates between (1) and (2) to obtain updated estimates of the complex gain corrections and the signal AOA.

3.2. Self-Calibration Algorithm of Manikas [2]

Unlike the algorithms of Flieller and many other authors whose work often centers around some modification or optimization of the MuSIC cost function [1]-[3], the algorithm in [2] takes the novel approach of formulating the problem of DF using an uncalibrated array in an H_∞ framework. Based on a state-space equivalent for the conventional array signal model, results from linear estimation in Krein space can be used to easily derive an H_∞ filter that removes the "uncertainties" of the array signal model that are otherwise manifest in the received signal. The H_∞ approach results in a minimization of the worst-case scenario. The algorithm is initialized with nominal values of the AOA supplied by an algorithm such as MuSIC. Based on the nominal AOA, the H_∞ filter is constructed, and the received signal is fed as the filter input. The filter output is then fed back into MuSIC to update the AOA estimate, and the process repeats itself. This routine, illustrated in Figure 1, leads in theory to an improved DF spectrum and hence a more accurate AOA estimate. However, it does not yield calibration gains, and is computationally intensive, especially since each iteration appeals to MuSIC, requiring an eigendecomposition.

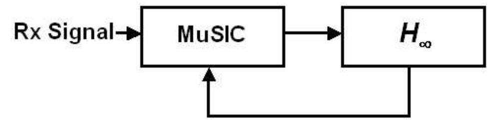

Fig. 1. Flow diagram for the Manikas algorithm.

4. EXPERIMENTAL RESULTS

Since the calibration source is in the near field of the array for the experimental data, a 2-D MuSIC DF search over range *and* azimuth AOA is required. Only the AOA is of interest here and therefore the range is treated as a nuisance parameter. An uncalibrated array is simulated from the data by introducing phase perturbations to each element of the nominally calibrated array as noted in Section 2.

Figure 3 shows a typical 2-D MuSIC spectrum for the source, when the calibration gains are subject to phase perturbations uniform on $[-80°, 80°]$ (the vertical line in each spectral plot shows the location of the ideal peak). Figure 4 and 5 show the results of applying the Flieller and Manikas algorithms, respectively, on the data used to generate Figure 1. It can be seen that while both algorithms significantly suppress the spurious peaks in Figure 1, the Flieller algorithm clearly does a superior job. Note that the actual spectrum magnitude in Figure 4 is substantially larger than the actual spectrum magnitude of Figures 3 and 5. However, all MuSIC spectra have been normalized so that the largest peak has unit magnitude, thus facilitating a direct comparison of side-lobe levels between figures.

Figure 6 shows the result of the average of a 50-trials Monte-Carlo simulation comparing the performance of the Flieller and Manikas algorithms when the calibration gains are subject to perturbations uniform on $[-\theta°, \theta°]$. It can be seen that the Flieller algorithm consistently yields more accurate azimuth estimates than the Manikas algorithm. It should be noted that both of the self-calibration algorithms begin to fail as the applied phase perturbations continue to increase towards $180°$. Neither algorithm succeeds on the experimental data directly without using any nominal calibration. It should also be noted that the data provides a high signal-to-noise ratio (SNR) test scenario; the receive array SNR is approximately 40-45 dB.

Although the Manikas algorithm offers no apparent advantage over the Flieller algorithm and little advantage over MuSIC (observe that in Figure 6, the azimuth error magnitude of MuSIC follows the Manikas algorithm closely) in high SNR scenarios, it is anticipated that the Manikas H_∞ "worst-case" design criterion should provide a performance advantage in a low SNR environment. To simulate a low

SNR environment, complex Gaussian white noise with standard deviation σ is added to the measured data. As shown in Figure 7, at a sufficiently high background noise level, the Flieller algorithm starts to exhibit worse performance than the Manikas algorithm. Note that in Figure 7, MuSIC exhibits performance similar to that of the Manikas algorithm at high SNR, but starts to resemble the Flieller algorithm in peformance as the SNR decreases. Figures 8 through 10 depict the dual of Figures 3 through 5 for the low SNR ($\sigma = 70$ V) scenario. It is clear that in the low SNR case, the Manikas algorithm does a much better job than the Flieller algorithm in suppressing spurious peaks.

From these experimental results, it is deduced that the Flieller algorithm offers good performance for practical scenarios in which average to high SNR levels exist. The Manikas algorithm is robust in that it has similar performance across a wide range of SNRs, though its ability to suppress spurious peaks is more pronounced in low SNR scenarios. This can be attributed to the H_∞ design criterion of the Manikas algorithm which sacrifices performance in scenarios with average to high SNR levels for improved performance in a "worst-case" low SNR environment.

5. SUMMARY

The ability of two self-calibration algorithms to estimate the AOA of an unsurveyed source using a surveyed but imperfectly calibrated array was evaluated using experimental data. It was shown that the Flieller algorithm outperforms the Manikas algorithm for high SNR and also has the advantage of outputting array calibration updates in addition to AOA estimates. The Manikas algorithm does offer a performance advantage in a low SNR environment, as anticipated from its H_∞ design criterion. For practical applications in which an array is initially calibrated and self-calibration is employed for calibration updates, high SNR signals of opportunity would most likely be used. The Flieller algorithm would thus be a better match to this application.

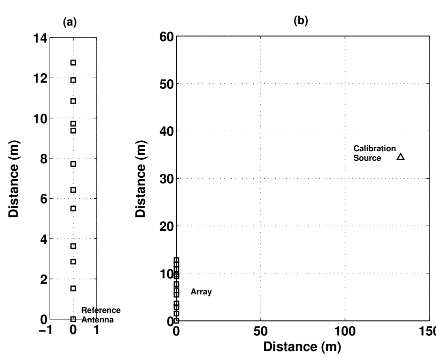

Fig. 2. (a) Array configuration (b) Experimental setup of calibration source with respect to the array.

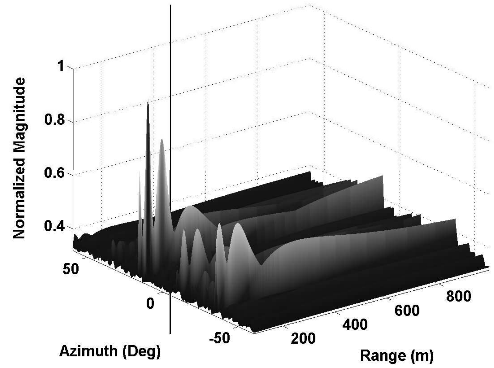

Fig. 3. 2-D MuSIC spectrum for source in *high* SNR environment with calibration phase errors on $[-80°, 80°]$

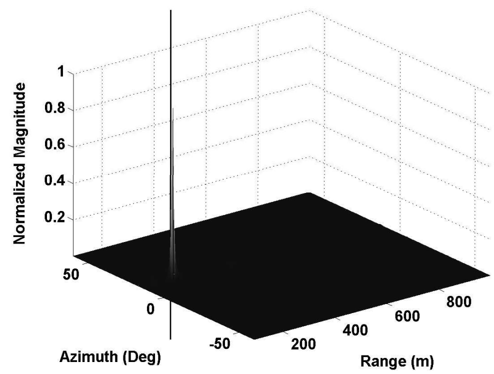

Fig. 4. 2-D MuSIC spectrum for source in *high* SNR environment after application of Flieller algorithm

6. REFERENCES

[1] A. Flieller et. al., "Robust bearing estimation in the presence of direction-dependent modelling errors: identifiability and treatment," *ICASSP-95,* pp. 1884-1887, May 1995.

[2] T. Ratnarajah and A. Manikas, "An H_∞ approach to mitigate the effects of array uncertainties on the MUSIC algorithm," *IEEE Sig. Proc. Let.,* vol. 5, pp. 185-188, Jul. 1998.

[3] A.J. Weiss and B. Friedlander, "Eigenstructure methods for direction finding with sensor gain and phase uncertainties," *Circ. Sys. Sig. Proc.,* vol. 9, pp. 271-300, Mar. 1990.

[4] G.H. Whipple, C.M. Keller, and K.W Forsythe, "Performance characterization of external array self-calibration algorithms using experimental data," *34th Asilomar Conf. Sig., Sys. Comp.,* pp. 623-628, Oct. 2000.

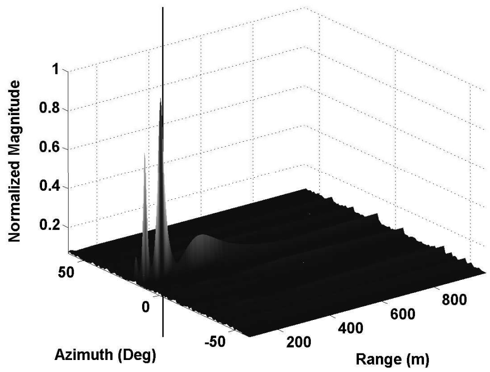

Fig. 5. 2-D MuSIC spectrum for source in *high* SNR environment after application of Manikas algorithm

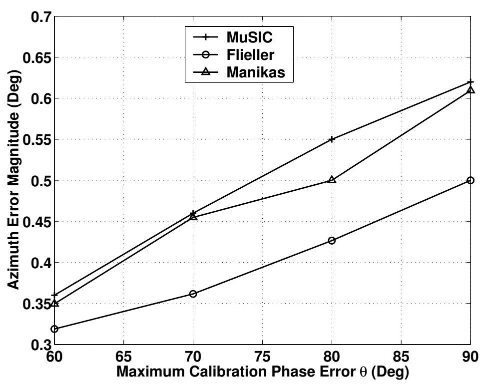

Fig. 6. Dependence of azimuth error on calibration phase errors, where calibration phase errors are uniform on $[-\theta^\circ, \theta^\circ]$

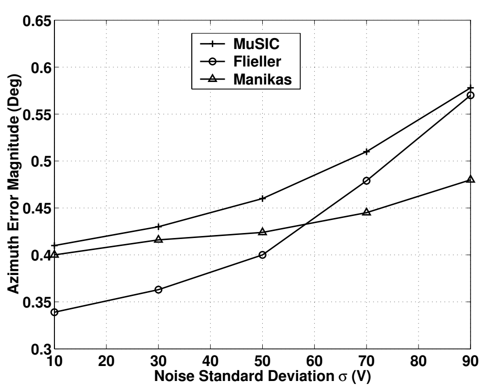

Fig. 7. Dependence of azimuth error on background noise level

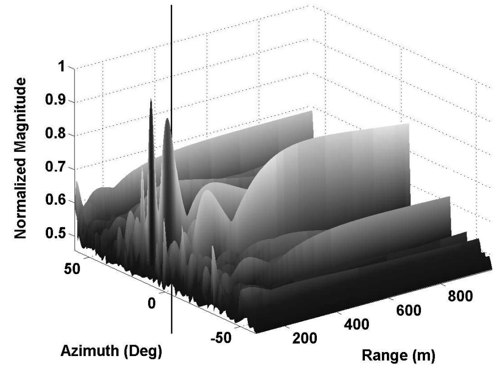

Fig. 8. 2-D MuSIC spectrum for source in *low* SNR environment with calibration phase errors on $[-80^\circ, 80^\circ]$

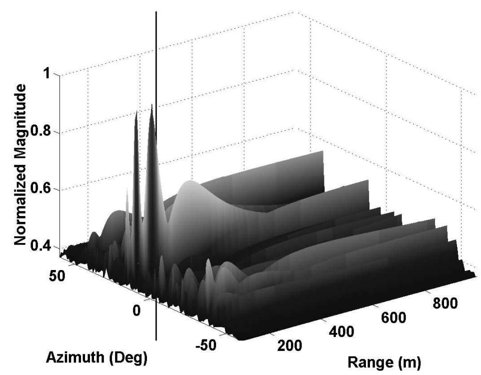

Fig. 9. 2-D MuSIC spectrum for source in *low* SNR environment after application of Flieller algorithm

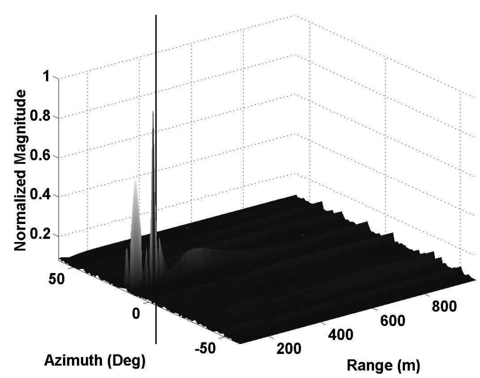

Fig. 10. 2-D MuSIC spectrum for source in *low* SNR environment after application of Manikas algorithm